On-Line Control of Crystal Properties in Nonisothermal Antisolvent Crystallization

Navid Ghadipasha and Jose A. Romagnoli
Dept. of Chemical Engineering, Louisiana State University, South Stadium Road, Baton Rouge, LA 70803

Stefania Tronci and Roberto Baratti
Dipartimento di Ingegneria Meccanica, Chimica e dei Materiali, Università degli Studi di Cagliari, via Marengo, 2, I-09123, Cagliari, Italy

DOI 10.1002/aic.14815
Published online April 13, 2015 in Wiley Online Library (wileyonlinelibrary.com)

The issues regarding the design and implementation of on-line optimal control strategies of crystal properties in nonisothermal antisolvent crystallization processes to control particles' mean size and standard deviation are dealt. The one-dimensional Fokker–Planck equation is used to represent the dynamic characteristics of the crystal growth and generate iso-mean and iso-standard deviation curves. Using controllability tools it is demonstrated that the system is ill conditioned in the whole operational range, posing limitations on the achievable control performance. To circumvent the problem, a control strategy is formulated by pairing crystals' mean size with antisolvent feed rate and manipulating temperature to control the standard deviation. A novel digital image-texturing analysis approach is discussed and implemented to track crystals' size distribution along the experiment and providing the on-line information for further feedback control action. Subsequently, alternative control strategies are implemented and tested to achieve a desired crystal size distribution. © 2015 American Institute of Chemical Engineers *AIChE J*, 61: 2188–2201, 2015
Keywords: nonisothermal antisolvent crystallization, image analysis, Fokker–Planck equation, neural network, real-time control

Introduction

Crystallization is the main physical separation process in many chemical industries. It is an old unit operation which can separate solids of high purity from liquids, and is widely applied in the production of food, pharmaceuticals, and fine chemicals. There are significant properties of the final product such as purity and stability of crystalline particles, growth morphology, and size distribution that affect downstream unit operations including filtration, granulation, and drying. Due to particulate form of crystals, size distribution is an important aspect of the end product which needs to be controlled. This physical textural feature influences solid properties such as filtration rate, bioavailability, and dewatering rate. Size distribution of crystals is very sensitive to various kinetic and thermodynamic parameters some of which are temperature, antisolvent flow rate, and seeding variables[1] that might change owing to unavoidable disturbances during the process. Hence, to fulfill the product specification it is important to properly control the physical reaction which necessitates understanding the dynamic of the system and underlying phenomena.

The driving force in crystallization process is the difference between chemical potential of the liquid phase and solid phase that can be closely related to supersaturation which is defined as the difference between the concentration of the solute in the mother liquor and equilibrium concentration. Common methods to achieve supersaturation are evaporation, cooling, and antisolvent addition. It is recently demonstrated that when cooling and antisolvent addition approaches are combined together, it could increase crystallization yield and improve product qualities including crystals' mean size.[2] Although system considered had solubility which was strongly a function of temperature, it has been shown even for systems with solubility weakly dependent on temperature; it is possible to impart significantly improved control over both distribution mean size and coefficient of variation by manipulating temperature together with antisolvent feed rate.[3] This plan would allow us to add a second degree of freedom (cooling) to be used to control the crystal size distribution (CSD).

Regarding the control of CSD, one typical approach used is based on model-developed optimal profiles which are then implemented on-line with or without any feedback (FB) action. Some examples of antisolvent crystallization modeling are paracetamol[4] and sodium chloride.[5,6] Recently, cooling has been combined with antisolvent crystallization and the joint process has been modeled for lovastatin[2] and acetylsalicylic acid.[7]

In contrast to model-developed optimal profiles, there has been alternative ways to control antisolvent and cooling processes. These have been supersaturation control,[8–11] and direct nucleation control.[12] In supersaturation control, the aim is to restrain the concentration of solute to keep

Correspondence concerning this article should be addressed to J. A. Romagnoli at jose@lsu.edu.

supersaturation at a constant low level to maximize crystal growth. The concentration is usually measured using attenuated total reflectance-Fourier transform infrared (ATR-FTIR).[13–16] It is the most widely used technique for concentration measurement during crystallization. Although the proposed approach has been shown to be robust and provide high control quality,[14–17] for unseeded crystallization large variability in product CSD was reported[17] which is due to the unpredictable nature of primary nucleation. Moreover, calibration of the instrument is very sensitive to impurities in calibration solutions.[18] Additionally, from an industrial viewpoint, mechanical damage, thermal stress or chemical deterioration of the ATR element immediately affects the calibration accuracy; and encrustation of the probe can easily occur which makes it difficult to apply ATR-FTIR in industrial crystallizers.[19]

In indirect nucleation control, the aim is to maintain the number of particle counts at a predetermined value using an on-line particle counter. In recent years, the application of focused beam reflectance measurement (FBRM) has gained popularity. In this method which is based on laser light scattering, online monitoring of the chord length distribution (CLD) of crystals is determined which is statistically related to the CSD. Several works on the application of FBRM in FB control of CSD are reported. Tadayyon and Rohani[20] investigated cooling crystallization of potassium chloride (KCl). It was shown that effective control of mean crystal size in the presence of set-point and disturbance changes is feasible. Abu Bakar[21] used the information on nucleation and dissolution from the FBRM in a FB control strategy to directly control the apparent onset of nucleation to achieve larger crystals with a narrow CSD and grow a desired polymorphic[22] form of crystals. For the FBRM technology, data are used more often qualitatively for monitoring the process because to restore the CSD from CLD, the geometry of the crystals must be well known and a three-dimensional model is also necessary to perform the time-consuming calculations.[23–25]

In this contribution, an image-based multiresolution approach to characterize CSD is embedded into an on-line FB control strategy to achieve a specific particle-size distribution. Crystallization of sodium chloride in water using ethanol as antisolvent is performed in an experimental bench-scale semibatch crystallizer. The proposed methodology utilizes the benefits of combining cooling and antisolvent to directly control both crystals' mean size and coefficient of variation. Using a novel stochastic approach as model to describe the time evolution of particle characteristics enables finding the explicit relationship between manipulated parameters (temperature and antisolvent feed rate) and controlled variables (mean size and standard deviation) and off-line determination of optimal trajectories. Furthermore, an operative map of the process is obtained, exploiting the availability of analytical solutions of the model. The operational map allows us to identify regions of input multiplicity which gives punctual information regarding stability of the process and regions of singularities. *In situ* measurement of crystals' size distribution using image-based technique and wavelet-fractal algorithm is implemented in a real-time environment for inferring the particles characteristics at different time of the experiment. Image-based technique is becoming increasingly more attractive due to availability of high speed imaging devices and powerful computers at reasonable costs and also the adaptability of this technique for real-time application. It is possible to detect single crystals in this method in case of touching and overlapping between particles which is inevitable during crystallization. Alternative control strategies are implemented and tested to attain a desired CSD. They include multiloop proportional integrals (PIs) approach, a feedforward (FF) strategy based on off-line calculated profiles, and a two stages control structure using a combination of FF and FB algorithm (FF/FB). Results demonstrate in some cases poor performance of the PI algorithm due to ill-conditioning of the process. Conversely, excellent behavior on the CSD control is achieved when the FF and the proposed FF/FB controllers are applied.

Theoretical Background

The recent development of a stochastic approach to model the nonisothermal antisolvent crystallization process of sodium chloride,[26–28] allowed an accurate analysis on the controllability property of such system. Different control strategies to track the system toward the desired CSD were compared by simulation using the nonlinear global stochastic model.[29] In this article, the experimental assessment and validation are performed to test the effectiveness of the alternative approaches. A brief description of the stochastic model and its use for the obtainment of the operational map and controllability properties of the system is reported in the following sections and will be used to select mean and standard deviation set-points and process conditions for the experimental testing.

Combined cooling and antisolvent crystallization modeling

The growth dynamic of a single crystal size L can be stated as a Langevin equation of the following type[26]

$$\dot{L}=Lg(L;\theta)+L\eta(t) \tag{1}$$

where $g(L;\theta)$ represents the growth rate with θ indicating the vector of model parameters, t is the time, and $\eta(t)$ is the Langevin force including the growth fluctuation. It is assumed that

$$E[\eta(t)]=0 \tag{2}$$
$$E[\eta(t)\eta(t')]=2\sqrt{D}\delta(t-t')$$

where, D is the noise intensity and represents the dispersion of the CSD. The dynamic behavior of the probability density distribution of the crystal size has been obtained by recurring to the Fokker–Planck equation (FPE) after performing a nonlinear variable transformation $y=\ln(L)$ in Eq. 1, and it is represented in Eq. 3

$$\partial_t\Psi=D\partial_{yy}\Psi-\partial_y[g(y,t;\theta)\Psi] \tag{3}$$

The FPE has to satisfy the following boundary Eqs. 4a,b and initial Eq. 5 conditions

$$\frac{\partial}{\partial y}\psi(-\infty,t)=0 \qquad \frac{\partial}{\partial y}\psi(+\infty,t)=0 \tag{4a,4b}$$

$$\psi(y,t_0)=\frac{1}{\sigma_0\sqrt{2\pi}}\exp\left[-\frac{(y-\mu_0)^2}{2{\sigma_0}^2}\right] \tag{5}$$

where μ_0 and σ_0 are, respectively, the initial mean size and standard deviation of crystals in logarithmic scale at $t=t_0$ which are determined experimentally.

The growth rate function in the variable y, allowing the most simple and accurate representation of the crystallization system is the logistic one[26] which is reported in Eq. 6

$$g(y;\theta)=ry\left(1-\frac{y}{K}\right) \tag{6}$$

Simple relationships have been developed in Cogoni et al.[28] to correlate the parameters r and K in Eq. 6 along with the noise intensity D in Eqs. 2 and 3 to the antisolvent flow rate and temperature

$$\begin{aligned} r(q,T)&=0.5264+0.5983q-6.4588\cdot 10^{-4}T \\ K(q,T)&=4.9176-0.0238q^2+1.7139\cdot 10^{-4}T^2 \\ D(q,T)&=0.2134+0.0277q^2-0.0019T \end{aligned} \tag{7}$$

Combining Eq. 3 with Eqs. 6 and 7, the stochastic model can be applied to the whole operating range of the experimental system.

Controllability analysis

The global model of the crystallization system can be used to analyze the input-output relationships to evaluate the process characteristics, such as stability and transient response. First, it is important to construct the operative map, where the two moments of the CSD at asymptotic conditions can be represented as a function of antisolvent flow rate and temperature.

The asymptotic mean, $\mu_{y,asymp}$, and variance, $\sigma^2_{y,asymp}$, definitions are provided as the first two moments of the distribution in Eqs. 8a,b, where Ψ_{asymp} represents the CSD at asymptotic conditions[29,30]

$$\begin{cases} \mu_{y,asymp}(q,T)=\displaystyle\int_{-\infty}^{+\infty} y\Psi_{asymp}(y;q,T)dy \\ \sigma^2_{y,asymp}(q,T)=\displaystyle\int_{-\infty}^{+\infty} \left(y-\mu_{y,asymp}(q,T)\right)^2\Psi_{asymp}(y;q,T)dy \end{cases} \tag{8a, 8b}$$

For the problem at hand, it is possible to analytically solve Eq. 3 at the stationary solution[30] obtaining the expression of the asymptotic distribution as

$$\Psi_{asymp}(y;q,T)=\frac{\exp\left[\frac{r(q,T)}{D(q,T)}\left(\frac{y^2}{2}-\frac{y^3}{3K(q,T)}\right)\right]}{\displaystyle\int_{-\infty}^{+\infty}\exp\left[\frac{r(q,T)}{D(q,T)}\left(\frac{y^2}{2}-\frac{y^3}{3K(q,T)}\right)\right]} \tag{9}$$

Choosing a mean size value, Eqs. 8a,b can be iteratively solved in the domain of the operating conditions to calculate all the possible standard deviations for that specific mean size. This allows constructing the asymptotic iso-mean (blue line) and iso-standard deviation (red line) curves reported in an antisolvent flow rate-temperature plane in Figure 1.

The operative map is used here to choose the target distributions in terms of mean and standard deviation, recalling that the two moments cannot be selected independently.

As demonstrated in Cogoni et al.[29] and pointed out in Figure 1, the underlying system exhibits input multiplicity. Therefore, it is possible to obtain the same asymptotic mean and standard deviation with two different couples of manipulated input values. This implies that the gain process may change sign making the system difficult to handle with conventional FB control.[31] The region in the (q,T) plane where the matrix of the process gain at asymptotic condition is singular is called catastrophe locus, and it has been shown with a black dashed line in Figure 1. From a control point of view where the gain array becomes singular, there is no direct guidance on the loop pairing between the manipulated and the controlled variables and a conventional control system may be inadequate if asymptotic conditions are lying on (or are close to) the singularity loci have been chosen as target values.[31]

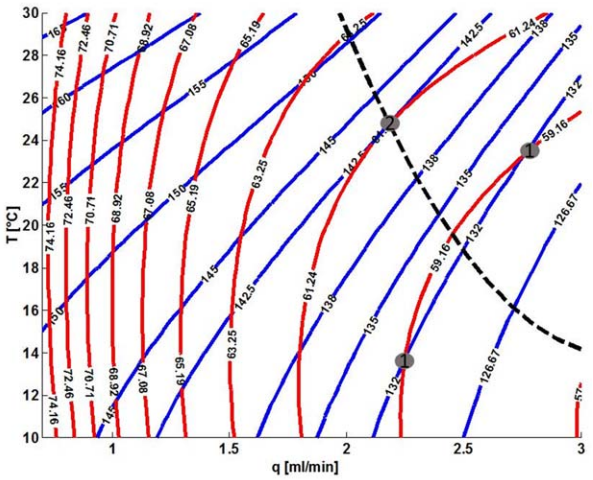

Figure 1. The isolevel curves represent, respectively, the asymptotic standard deviation (solid red lines) and the mean size (solid blue lines).

The catastrophe locus is reported as dashed black line. [Color figure can be viewed in the online issue, which is available at wileyonlinelibrary.com.]

As illustrative examples to consider different behaviors of the dynamical system, two asymptotic conditions are chosen as targets, which are: $(\mu,\sigma)=(132\mu m, 59.16\mu m)$ and $(\mu,\sigma)=(142.5\mu m, 61.24\mu m)$. According to the operational map, these points are feasible and the second one is on the catastrophe locus of the system as shown by gray circles in Figure 1. These two set-points will be considered later during the implementation and testing alternative control strategies.

Experimental Section and CSD Characterization

Experimental set up and procedure

Crystallization of sodium chloride in water using ethanol as antisolvent is considered as the case study. Reagent grade sodium chloride (NaCl) of 99.5% purity (Sigma-Aldrich), 190 proof ethanol provided by Pharmco-AAPER and only purified water are used during the experiment. The initial solution consists of 34 g NaCl in 100 g of deionized water. The experimental rig (Ace Glass Incorporated) is made up of 1 L glass, jacketed cylindrical crystallizer, connected to a heating/cooling bath controller. The temperature in the crystallizer is measured using an resistance temperature detectors (RTD) probe which is wired up to a slave temperature control system (Thermo Fisher Scientific) capable of heating and cooling. Mixing is provided by a magnetic stirrer at the speed of 400 RPM. In similar fashion, the antisolvent addition is performed using a calibrated peristaltic pump (Masterflex Model 77200-60, Cole-Parmer). The master control is performed by a computer control system which is connected

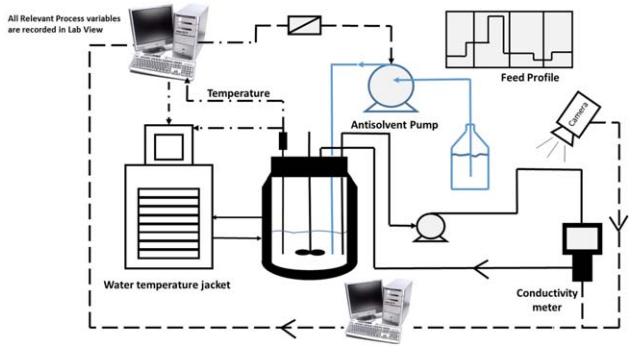

Figure 2. Schematic of apparatus and sensors used in this work.

[Color figure can be viewed in the online issue, which is available at wileyonlinelibrary.com.]

to the slave temperature and flow rate controllers respectively. The desired set-points are set by the master controllers.

Along the experiment, particles are circulated throw a second pump (Masterflex Model 77200-60 Cole-Parmer) into a cell where they are lighted up by an illumination system. Images are taken continuously using a universal serial bus (USB) microscope camera (BASLER make, Model MD900) which fits into the side tube on the side of the microscope with one of the supplied adapters and connects to a dedicated computer. Using image-based texture analysis, CSD, that is, mean and standard deviation are determined. During implementation of any FB controller the results are compared with the desired set-points. Applying a proper control plan, the error is used to calculate the value of temperature and the amount of antisolvent flow rate (set-points). Data is then sent to the data acquisition and control computer running Labview (2009). The software is linked to the pump and the heating/cooling bath so the updated values are applied in the plant. All the experimental set up and instrumentation are displayed schematically in Figure 2.

As part of our experimental investigation, on-line monitoring of the solute concentration was also implemented. This additional measurement will not be used specifically in the control program but provide practical information regarding solute mass transfer and the rate of crystal mass evolution as well as allowing us to analyze the performance of alternative control strategies discussed in this article. In this work, the concentration of the solution is measured by simultaneously evaluating the solution conductivity, antisolvent mass fraction, and temperature. A similar measurement for Ammonium sulfate is reported by Abbas[32] and Nowee.[33] This procedure states an inferential measurement whereby the conductivity, antisolvent mass fraction, and temperature are the primary measurements which are then translated into the secondary inferred measurement being the concentration. Conductivity is gauged on-line using an Orion 4 STAR conductivity probe model 018020 MD.

Solubility of NaCl is assumed to be independent of temperature in the small ranges. However, the conductivity of a solution increases with temperature, as the mobility of the ions increases.[34] If the temperature T does not vary too much, a linear approximation is typically used

$$\delta(T)=\delta_0\ [(1+\alpha(T-T_0)] \tag{10}$$

$\delta(T)$ is the conductivity at the measured temperature in mS/cm, α presents the temperature coefficient of resistivity, T_0 is a fixed reference temperature (20°C for this experiment), and δ_0 is the conductivity at the reference temperature T_0. The parameter α is fitted from measurement data. Equation 10 is used to convert the conductivity of the solution at the temperature of the experiment to the value at the reference temperature (20°C) where it can be transformed to concentration. At 20°C a series of solutions of aqueous ethanol at known concentrations (10, 20, 30, 40, 50, 60, 80 wt %) are prepared representing the concentration range of the crystallization experiment. The conductivities of these solutions are measured at various salt concentration range of crystallization. The data collected are shown in Figure 3. As it can be observed, the conductivities of the various solutions increase until a point where it becomes independent of concentration. In fact, when solubility equilibrium is reached, the rest of the salt that is added to the solution is deposited at the bottom of reactor and does not contribute to the concentration of ions. As the effect of salinity on dielectric constant and viscosity is negligible,[35] according to Debye–Huckel–Onsager theory, ions' concentration is the only factor that influences the conductivity of the solution which is constant after equilibrium point. This point illustrates the limiting conductivity at which any further increase is only possible by decreasing the ethanol weight percent. The locus

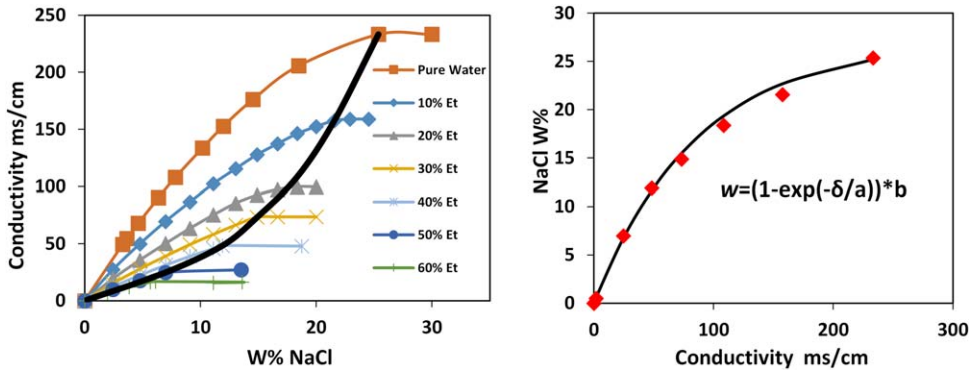

Figure 3. Conductivity of sodium chloride at various concentrations and ethanol mass fraction (left Panel) with the equation shown for the locus of limiting conductivity vs. sodium chloride mass percent (right panel).

[Color figure can be viewed in the online issue, which is available at wileyonlinelibrary.com.]

of these points is tracked as an exponential model of concentration as a function of conductivity (Figure 3)

$$w = \left(1 - \exp\left(-\frac{\delta_0}{a}\right)\right) * b \tag{11}$$

a and b are constants with values 86 and 27, respectively, for this case study. This equation is used to determine the salt weight percent at the measured conductivity which can then be converted to concentration knowing the amount of antisolvent added and the total volume of the solution.

In situ crystal size distribution measurement

The control strategies proposed in this work use the mean crystal size and standard deviation of the CSD estimated by a sensor recently developed by Zhang.[36,37] This technique is based on image processing of the crystals, and it is able to extract the required information on textural properties irrespective of whether it is applied to single particles or clusters. In this method, which is based on combining thresholding and wavelet-fractal-energy algorithm, images are considered as a two-dimensional array of pixels with various intensities. Otsu's global thresholding method and an optimum threshold value for the intensity can be exerted to identify the intensity of crystal edges and remove the background. In this way, location of crystal clusters that have different intensities from the background can be detected and the information regarding intensities of those points will be restored into a vector. Discrete wavelet transformation (DWT) is then applied to the signal obtained by processing the image. DWT extracts textural characteristics of crystals by decomposing the signal into several details, which are crystals' edges in our case and an approximation, called the intensity variance caused by illumination. The new information in terms of variance of wavelet coefficients are further processed to obtain the fractal dimension (FD). This last property has been selected as texture feature as it has been demonstrated that dynamics of crystal growth follows fractal process.[38] An artificial neural network is then designed using the texture information (FD, energy signatures for details level from 2 to 5) in conjunction with the available on-line process conditions (flow rate, temperature, and time) as inputs for the estimation of the crystal properties (mean size and standard deviation) as output in the whole operating range.

A complete automated laboratory scale software/hardware framework for capturing crystal images, texture analysis, and final prediction of the CSD was implemented for the on-line measurement. The experimental setting utilizes a USB microscope camera (model MD900) with a resolution of 1280 × 960 pixels. The AMSCOPE software captures images for manual measurement to analyze particles individually. The magnification used is 25×, corresponding to 0.775 Microns/pixel. Images are taken at different crystallization stages that correspond to the selected sampling time. At each crystal growth step, a set of at least 10 images capturing different amount of crystals are applied. The original grey crystal image in tagged image format (TIF) format is imported for image analysis. It is compressed and cropped with Microsoft Office Picture Manager into a size of 960 × 1280 in JPG format to improve execution time for further analysis. The cropped image is then imported into MATLAB for image analysis, wavelet analysis, and artificial neural network (ANN) estimation. To make calculations simpler, the image intensities are normalized with intensity value into a range of 0–1. Figure 4, illustrates the predictions capabilities of the image-based CSD distribution during one of the batch runs, and the manually measured mean crystal size is compared with the one estimated by the neural network model.

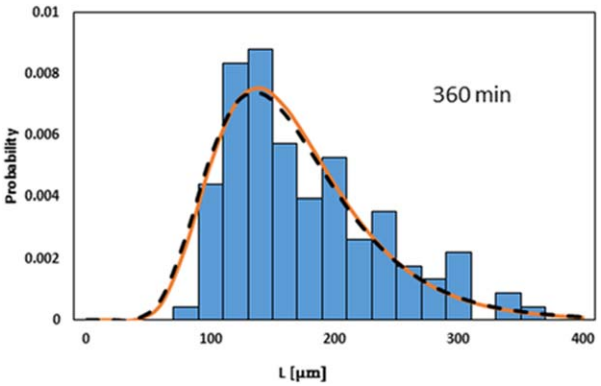

Figure 4. Comparison between estimated CSD (dashed line), raw histogram, and the smoothed approximation with the manually measured distribution parameters at one sampling time from the crystallization batch run.

[Color figure can be viewed in the online issue, which is available at wileyonlinelibrary.com.]

Fitting of experimental histogram

The different control algorithms proposed in the following sections will be compared in terms of mean and standard deviation of the crystal size estimated at different sampling time, and also considering the CSD at the end of the batch. For the latter, a number of images are taken and manually analyzed to produce the corresponding histogram. This representation of the experimental results requires that a very high number of crystals be considered to adequately describe the population of crystals, with a prohibitive effort for the experimentalists. The knowledge of the type of distribution for the crystal size, along with a practical number count allows the obtainment of a good representation of the experimental CSD. According to previous studies,[39] a log-normal distribution is considered as best fit of the experimental data obtained at the end of the batch for the different runs. One of them is reported as illustrative example in Figure 5, where the log-normal approximation is compared with the histogram of the relative frequency density of the crystal sample along with the kernel approximation (nonparametric fitting). Being the two continuous curves almost overlapping and considering that no assumption is made for the nonparametric approach, the log-normal assumption is assumed to be valid and also the number of samples can be considered sufficient for a good representation of the experimental CSD. In the following, the results obtained with the parametric fitting will be shown, but in case of system behavior exhibiting different distribution, as in case of multimodal CSD, a nonparametric representation is more adequate.

On-line control of the crystal size distribution

Different control schemes have been applied to the crystallization system to achieve a desired asymptotic CSD by controlling antisolvent flow rate and temperature. For the present system, the target CSD could be assumed lognormal,[39] and it is characterized by selecting a proper mean and

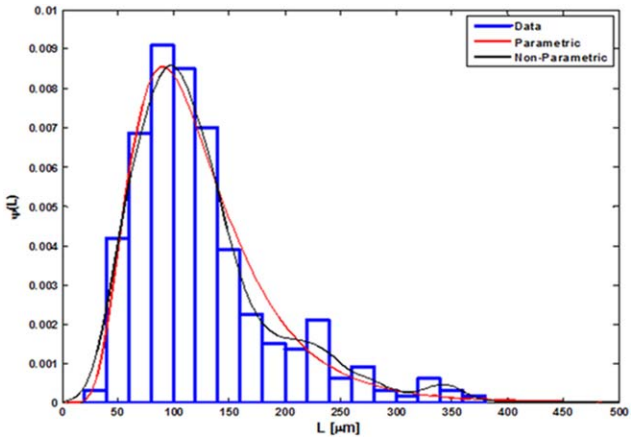

Figure 5. Comparison between parametric and nonparametric fitting calculated with data at the end of the batch for the experimental run using PI controller and $(\mu,\sigma)=(132\ \mu m,\ 59.16\ \mu m)$ as set-point.

[Color figure can be viewed in the online issue, which is available at wileyonlinelibrary.com.]

standard deviation. Target selections have been conducted exploiting the model of the process presented in controllability analysis section and its operating map (Figure 1). In the following three different approaches are applied and discussed in the light of the experimental results.

Control algorithms

The first strategy applied is a conventional FB, where two loops are considered to control mean and standard deviation of the CSD by, respectively, manipulating flow rate of the pump and crystallizer temperature. The FB control uses a PI-like algorithm, which is expressed mathematically as follow

$$u_n=u_{n-1}+k_c\left[e_i+\frac{\Delta t}{\tau_i}\sum_{i=1}^{k}e_i\right] \tag{12}$$

where u_n denotes the value for input variables (temperature and flow rate) at each time instant which provide the set-points for the pump and heating/cooling system. k_c and τ_i illustrate the proportional gain and integral time constant of the controller. The errors in this formulation are given as the difference between the measured and target values for the mean and standard deviation of the CSD. The control scheme that fulfills the desired standard deviation of the crystals has a cascade structure comprised of two proportional-integral loops. The primary loop minimizes the error between current value of standard deviation and the target to specify the reactor temperature and the output is then used as a set-point of the thermobath to adjust the cooling/heating flow rate of the jacket to ensure the crystallizer temperature is satisfied. Concerning particles' mean size the determined antisolvent feed rate by the primary FB loop is sent to the pump and specifies the pump speed via a calibration block that has already been implemented in Lab View which relates the antisolvent flow rate to the pump speed in RPM.

As an alternative to the 2 × 2 PIs structure discussed before, an open-loop (FF) control is also implemented. This approach is introduced because eliminating FB action should avoid the problems related to ill-conditioning of the gain array matrix[29] and time-varying characteristics of the system.[40,41] The latter aspects imply that using a linear FB control ignores the fact that controller parameters should be adapted, as process moves along the given path. The FF approach has the potential to provide minimum residual area but will not be able to compensate if any disturbance hits the process or in case of model-plant mismatch, as no FB action is deployed. Consequently, a two-stage controller (FF/FB) has been also executed, where a FF strategy is combined with a FB controller (FB). In particular, the FF action is used to bring the system close to the asymptotic condition at around 5% of the desired set-point, and then the PI controller is activated to remove the offset for the crystals' mean size. As it will be observed, by relinquishing strict control on standard deviation it is possible to have a more efficient control on particles' mean size avoiding problem related to ill-conditioning if they should arise. A schematic representation of all the control configurations explored is given in Figure 6.

For the whole configurations analyzed in the following, the initial conditions of the batch are chosen to promote nucleation and speeds up the mean crystal growth rate. These conditions are maintained for 30 min and then the selected controller is switched on. Images are started to capture at this time and at each time step mean size and standard deviation measurements of the system are compared with the set-points.

Results and Discussion

The performance of the three types of controller will be analyzed considering two different cases, which differ from the position of the mean and standard deviation set-points in the (q, T) plane. Case 1 considers the targets far from the catastrophe locus (point 1 in Figure 1), whereas Case 2 set the target values belonging to the catastrophic locus (point 2 in Figure 1).

Case 1: Set-points far from the catastrophe locus

First, the results concerning the performance of the conventional FB control are discussed. In this case, the mean crystal size and standard deviation are controlled using two PIs which manipulate, respectively, the pump flow rate and system temperature. Parameters of the controller are tuned using different simulations carried on with the FPE model and sensible values for the proportional and integral constants for both structures are chosen for the experiments (Table 1). The sampling time was selected at 15 min for both the PI controllers, such as enough time is given to the

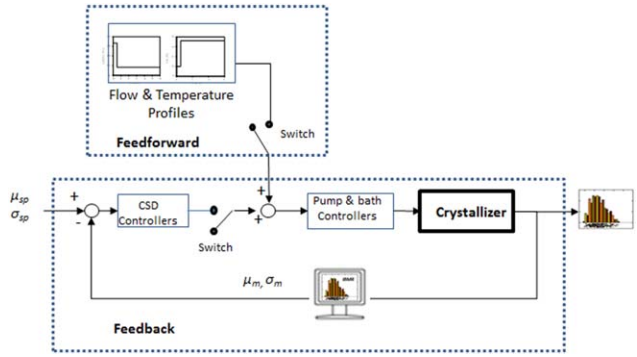

Figure 6. Schematic representation of possible control configuration.

[Color figure can be viewed in the online issue, which is available at wileyonlinelibrary.com.]

Table 1. Simulation Parameters for the Calculation of Temperature and Antisolvent Addition Policies

Tuning Parameters	K_c	τ_i
Flow rate	0.01	0.008
Temperature	0.04	0.1

CSD sensor to perform the image processing steps and the maximum heat exchangeable from the cooling/heating bath to vary temperature is respected.

The initial conditions of the batch are the highest flow rate (3 mL/min) and lowest temperature (10°C) to promote nucleation and speed up crystal growth. These conditions are maintained for 30 min and then the FB controller is introduced. Results are reported for a target CSD expressed as $(\mu, \sigma) = (132\ \mu\text{m},\ 59.16\ \mu\text{m})$. Figure 7 illustrates the size evolution of the crystals and the manipulated variables trajectories during the whole batch. At the beginning of the experiment, the flow rate is high and it cuts down to a lower value to promote crystal growth instead of the new crystal formation. After 2 h when the mean size exceeds its set-point value, flow rate increases to favor more crystal formation and a lower mean size. Although there is a large overshoot in the mean crystal size profile, the controller is able to bring the system to the desired mean value after about 5 h. The standard deviation exhibits larger fluctuations within the first hour and a half, due to an aggressive action of the controller, then it has smaller oscillation around the set-points and finally it maintains a small offset.

Using the global model described in Theoretical Background Section, a FF controller has been designed and applied to track the crystallization system to the desired set-points defined previously. Again, the beginning of the batch has been conducted at the highest antisolvent flow rate and lowest temperature allowable by the instrumentation. At time equal to 30 min, the manipulated inputs are moved to the values obtained by solving the nonlinear global model at asymptotic conditions for the selected mean and standard deviation values (Eqs. 8 and 9). A step function should be used as optimal trajectory as it allows reducing the integral error calculated as difference between output trajectories and target values.[29] This variation can be obtained with the antisolvent flow rate, but temperature follows a ramp due to the heat exchangeable rate from the cooling/heating bath (Figure 8). The outputs' behavior is reported in the bottom of Figure 8, which shows a rapid convergence of the mean and standard deviation to the set-points with only a small offset for the latter.

It should be remarked that this result is due to the availability of a very accurate model, but in case of disturbances or error mismatch, the FF controller would not be able to compensate for it. For practical application a two-stage controller is suggested, where the first part of the batch is conducted using the FF action and a PI controller is switched on toward the end of the run to perform final adjustments of the mean crystal size. In the proposed control plan, the FB loop is closed when the mean size is circa 5% of the set-points. The results obtained with the two-stage controller are reported in Figure 9 and they show that perfect control can be obtained for crystals mean size, without offset. It is worth noticing that using the FB only when it is close to the set-point allows the achievement of asymptotic conditions at about 1 h faster when compared with the conventional FB controller (Figure 7).

A more detailed analysis of the results can be acquired using the experimental distributions at the end of the batch. Figure 10 illustrates the asymptotic CSD distribution for the different runs under all controllers when compared with the set-point

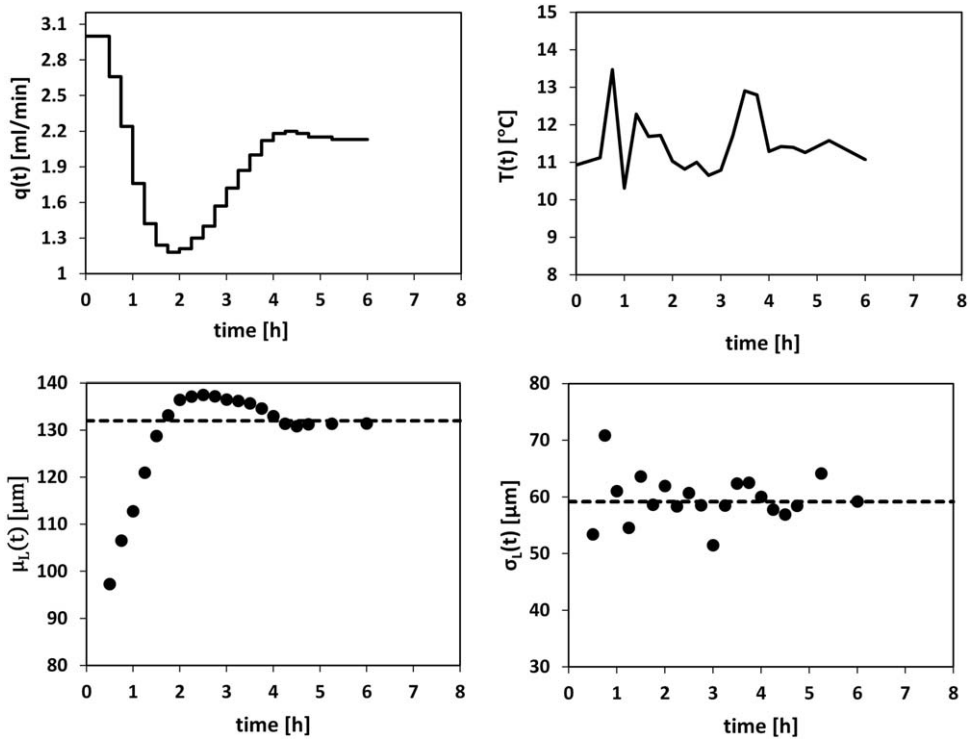

Figure 7. Manipulated and control variables profiles for PI controller.

Upper panel—Antisolvent flow rate (left) and temperature (right) profile. Bottom panel—evolution of mean (left) and standard deviation (right).

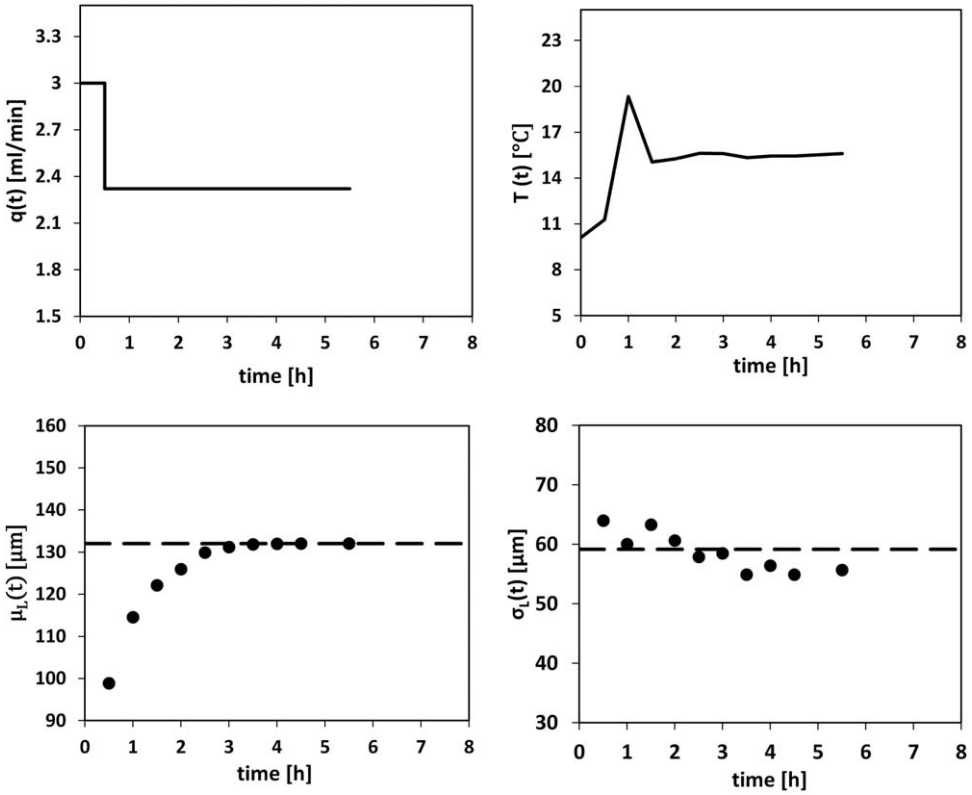

Figure 8. Manipulated and controlled variables profiles for FF controller.

Upper panel—Antisolvent feed rate (left) and temperature (right) profile. Bottom panel—evolution of mean (left) and standard deviation (right) for the set-point $(\mu, \sigma) = (132\mu m,\ 59.16\mu m)$.

distribution, where the experimental distribution have been fit with a log-normal function with the parametric approach described before. All the controllers exhibit good results in terms of final distribution, with slightly better performance for the FF controller, followed by the two-stage controller.

As further information on the controlled system it is important to represent the behavior of the salt concentration in the solution during the batch, as it may give indication on the nucleation/growth process when different input trajectories are implemented. The experimental data are shown in Figure 11 for the three control configurations with the sampling time of 15 min. Although the results show similar trends, there are some differences toward the end especially between the PI controller and both FF and FF/FB controllers. The similarities can be explained by the fact that all controllers attempt to produce a step change in the antisolvent flow rate toward the asymptotic value as indicated in the operating map. In the case of the PI controller this is achieved by small steps thus also producing an overshoot in the antisolvent flow rate which is later corrected (indicated also for the differences in the salt concentration toward the end). Furthermore, all the controllers exhibit similar good results in terms of final distribution, thus making sense on the similar "overall" behavior of the salt consumption.

Case 2: Set-points belonging to the catastrophe locus

The different control configurations described above have also been tested for the case when the targets belong to the catastrophe locus. The point is indicated in Figure 1 and it has the following mean and standard deviation values:$(\mu, \sigma) = (142.5\,\mu m,\ 61.24\,\mu m)$. This choice aims to assess the control configurations in a more demanding situation with respect to the previous one, because of the singularity in the input-output relationships.

First, the results obtained when using the PI controllers are shown in Figure 12, where controlled outputs, manipulated inputs, experimental distribution at the end of the batch and salt concentration profile are reported. Identical to the previous case, the batch starts using highest antisolvent flow rate ($q = 3$ mL/min) and lowest temperature ($T = 10°C$). As shown in Figure 12, the controller is not able to reach the final target indicating an off-set in the final values of the mean size, whereas the fluctuation in the standard deviation can be considered within the estimation error of the on-line sensor. It is interesting to note that antisolvent flow rate and temperature exhibits a large variation approaching the end of the batch, but with little effect of the crystal size. This fact can be explained by considering that salt concentration rapidly decreases and it is very low after 3 h from the beginning of the batch. The consumption of salt, due to the initial high antisolvent flow rate, makes the action of the controller useless as there is not sufficient salt even if the final CSD is quite satisfactory.

To test the controller performance at the end of run, using different initial conditions it is possible to diminish the consumption of salt at the first stage of the runs. Therefore, the next run has been conducted starting from an antisolvent flow rate value equal to 1.5 mL/min and a temperature value of 20°C. The results are reported in Figure 13, where the inputs and outputs behavior are shown along with the distribution at the end of the batch and the salt concentration. In

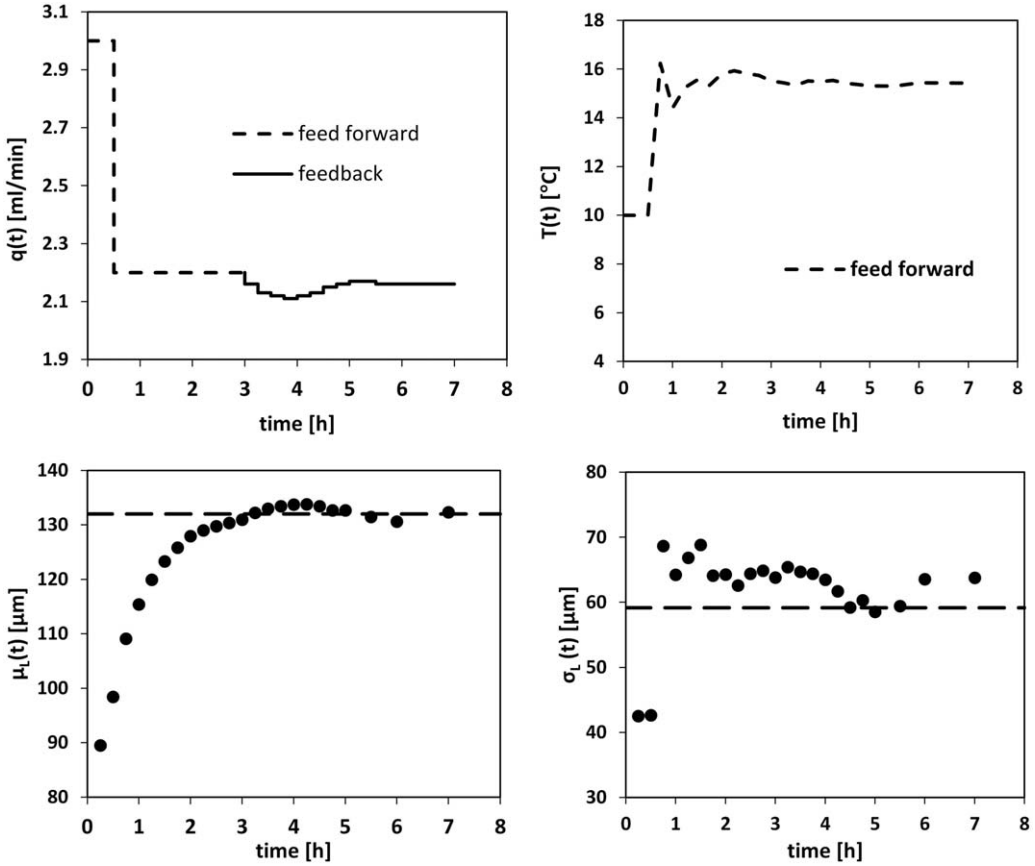

Figure 9. Manipulated and controlled variables profiles for FF/FB controller.

Upper panel–Antisolvent flow rate (left) and temperature (right) profile. Bottom panel—evolution of mean (left) and standard deviation (right) for set-point $(\mu,\sigma)=(132\mu m,\ 59.16\mu m)$.

this case the PI controllers are able to track the system to the desired set-points, thanks to the presence of a higher salt concentration within the first 3 h of the run. To adjust the mean crystal size, the antisolvent flow rate is increased after 2 h and a half to its maximum value by the controller, because it is favored the creation of new nuclei lowering the mean of CSD. However, the analysis of the shape of the final distribution (bottom of Figure 13) as given by the images taken at the end of the batch. As demonstrated, the final distribution is bimodal showing the effects of secondary nucleation with small crystal created at the end of the run. This can also be observed by analyzing the images, where small particles are observed jointly with the large particles already created (Figure 14). Consequently, even if the PI controller appears to achieve the control targets in terms of mean and standard deviation, it is not able to bring the

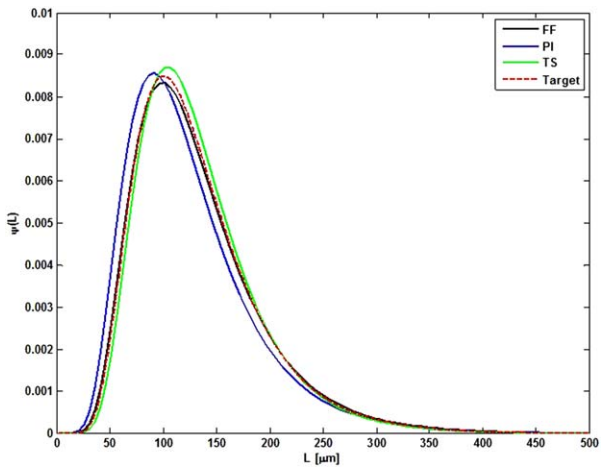

Figure 10. End of the batch distribution $(\mu,\sigma)=(132\mu m,\ 59.16\mu m)$ for all controllers.

[Color figure can be viewed in the online issue, which is available at wileyonlinelibrary.com.]

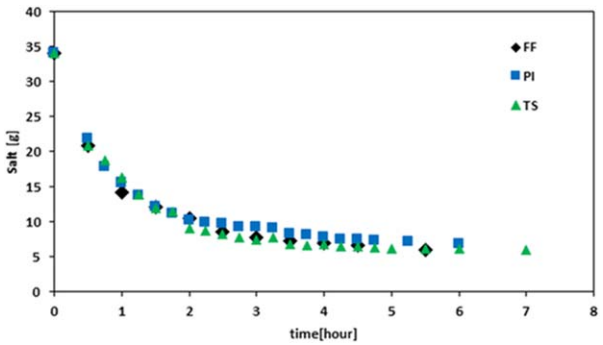

Figure 11. Salt concentration profile during run for set-point$(\mu,\sigma)=(132\mu m,\ 59.16\mu m)$ using FF, PI and FF/FB controller.

[Color figure can be viewed in the online issue, which is available at wileyonlinelibrary.com.]

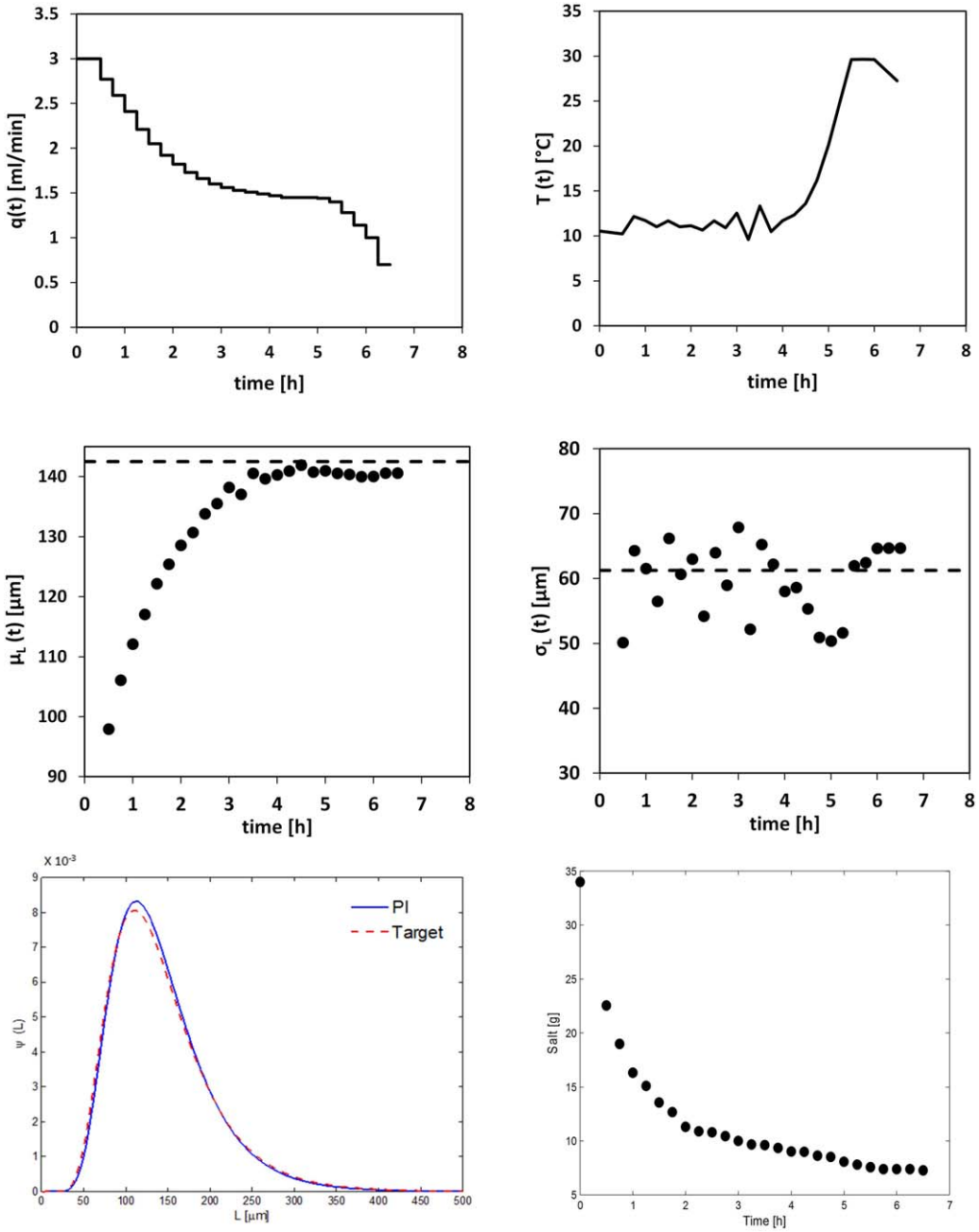

Figure 12. System behavior for PI controller with the initial condition of 3 ml/min and 10°C for set-point $(\mu, \sigma) = (142.5\,\mu m,\ 61.24\,\mu m)$.

Upper panel—Antisolvent flow rate (left) and temperature (right) profile. Middle panel—response of mean (left) and standard deviation (right) Bottom panel—End of the batch distribution compared with target (left) and salt concentration profile during run (right). [Color figure can be viewed in the online issue, which is available at wileyonlinelibrary.com.]

system to the target CSD (unimodal log-normal distribution with a specified mean and variance).

The poor performance of the conventional PI when operating close to the ill-conditioned region confirms what evidenced in the previous studies.[29] According to the simulation results by Cogoni et al.[29] the control problem can be approached using the FF action. Two runs have been conducted with this controller, one uses highest flow rate and lowest temperature during the first 30 min, then changing by a step to the input values calculated by means of the model and represented in Figure 1 (point 2). Then, an experiment has been conducted starting from the antisolvent flow rate and temperature values leading to the required asymptotic mean and standard deviation. In Figure 15, only the results obtained at constant conditions are reported, in the understanding that the behaviors of the system in the two cases are very similar. The performance of the controller is very good, with a small mismatch for the standard deviation, but the gap is within the estimation error of the sensor. The target has been obtained in this case also in terms of end of batch distribution, which is quite close to the desired log-normal CSD.

A further experiment has been conducted to test the system, when either disturbances and/or modeling errors are present and a FF action cannot assure offset-free

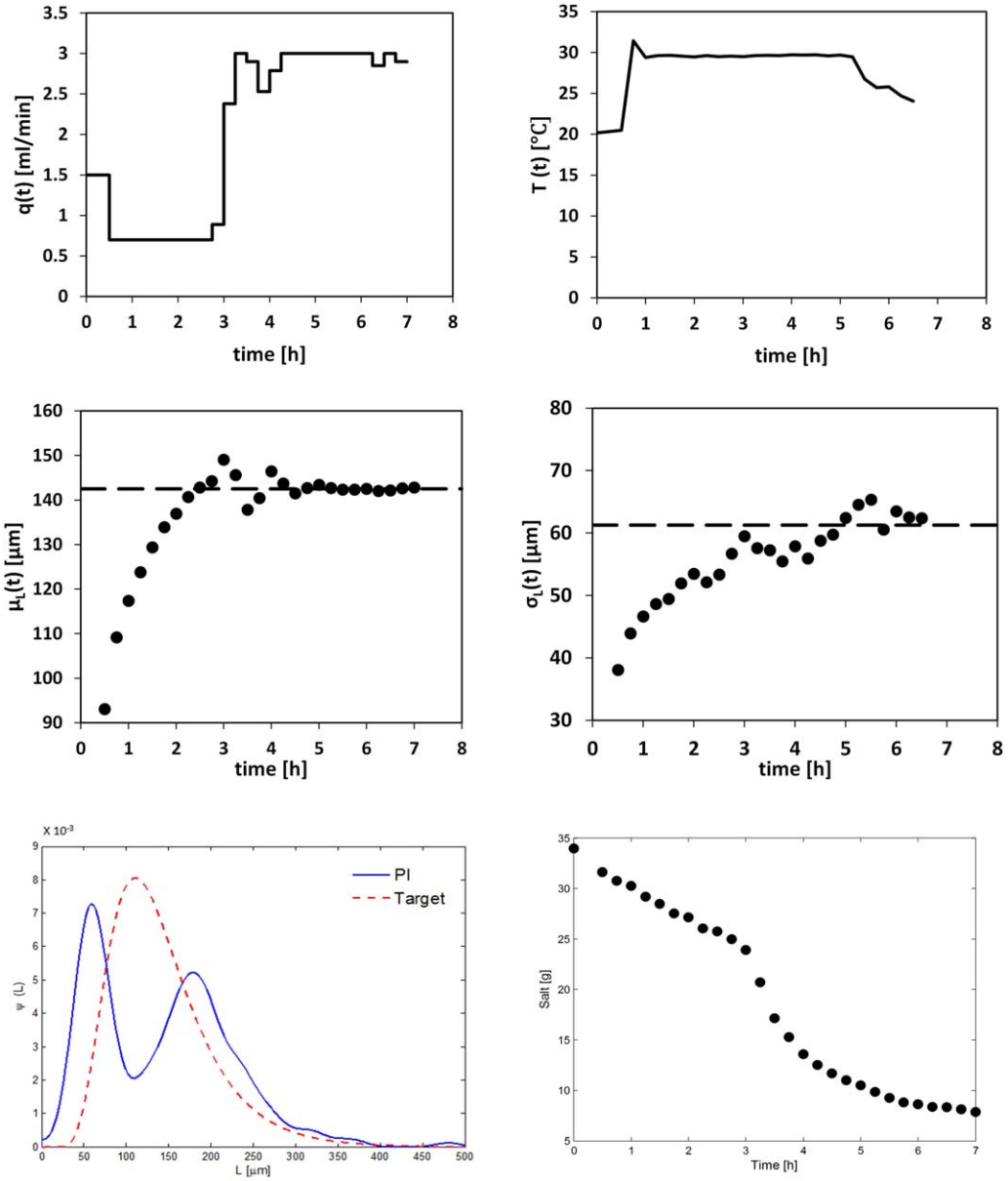

Figure 13. System behavior for PI controller with the initial condition of 1.5 mL/min and 20°C for set-point.

Upper panel—Antisolvent flow rate (left) and temperature (right) profile. Middle panel—response of mean (left) and standard deviation (right) Bottom panel–End of the batch distribution compared with target(left) and salt concentration profile during run(right). [Color figure can be viewed in the online issue, which is available at wileyonlinelibrary.com.]

performance. To accomplish this task, an error in the model estimation of antisolvent flow rate was introduced, and it is set equal to 1.8 mL/min instead of 2.1 mL/min. This situation may also represent a calibration error in the feed pump. As presented previously the FF control action is coupled with a PI controller (FB) which is switched on toward the end of the batch to perform final adjustments for the mean size (5%of the final mean size). The performance of the two-step controller are rather good and very close to the results obtained with the FF strategy, both in terms of the two moments and considering the shape of the distribution at the end of the batch, as shown in Figure 16. This clearly shows the importance of a FF/FB combination for realistic situations due to presence of unexpected disturbances. The proposed combination is able to perform a final correction eliminating the expected offset of an inherent open-loop controller when confronted with model and process disturbances.

Conclusions

An on-line strategy to directly control CSD in joint cooling antisolvent crystallization processes was proposed. Crystallization of sodium chloride in water using ethanol as antisolvent was performed in an experimental bench-scale semibatch crystallizer. A stochastic approach in the form of one-dimensional FPE was used to model the crystals' size distribution dynamic and for off-line determination of optimal trajectories in terms of manipulated parameters (temperature and antisolvent feed rate) and controlled variables (mean size and coefficient of variation). Furthermore, the explicit relation between inputs and outputs was obtained to sketch the operating map of CSD at asymptotic condition allowing us to identify regions of input multiplicity which gives punctual information regarding stability of the process and regions of singularities. The operating map was then used to select the

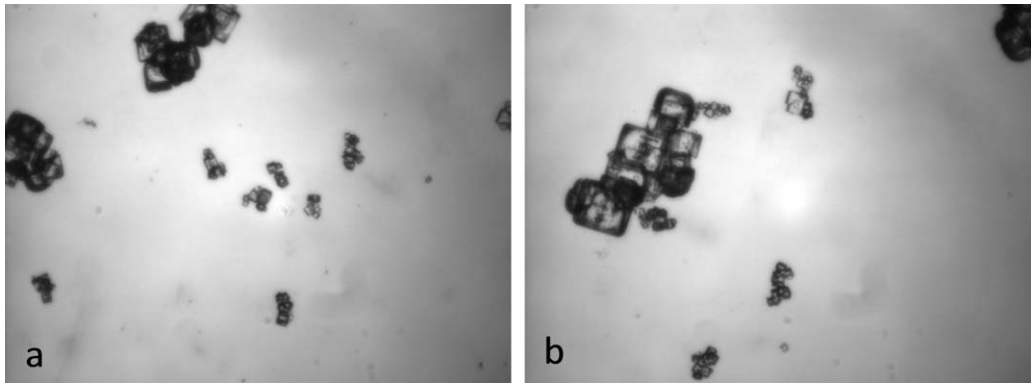

Figure 14. Sample images refer to $t = 390$ min.

The effect of secondary nucleation appears as small particles beside the big crystals that have already been formed.

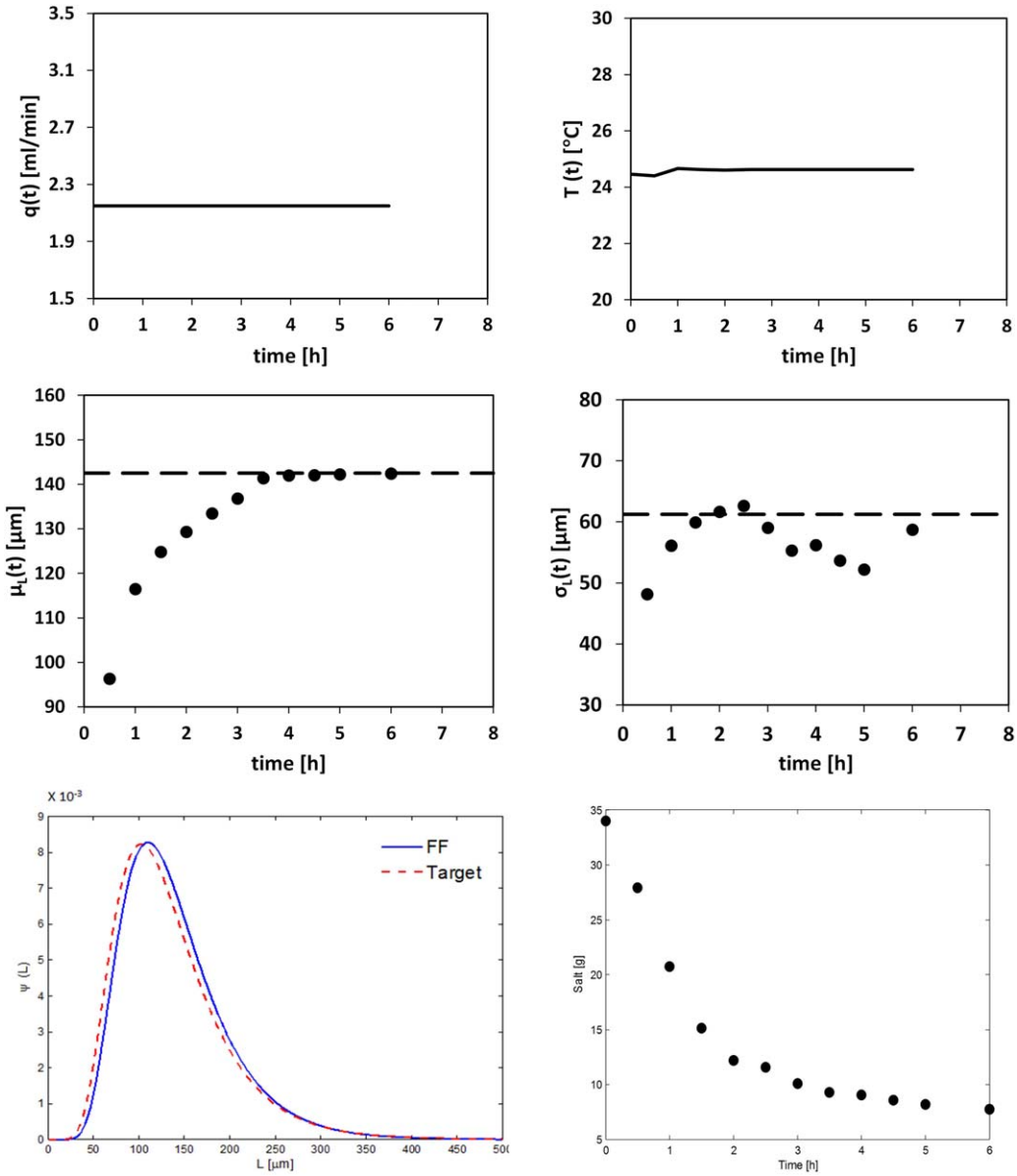

Figure 15. System behavior for FF with the initial condition of 2.1 mL/min and 24°C for set-point.

Upper panel—Antisolvent flow rate (left) and temperature (right) profile. Middle panel—response of mean (left) and standard deviation (right) Bottom panel—End of the batch distribution compared with target (left), and salt concentration profile during run (right). [Color figure can be viewed in the online issue, which is available at wileyonlinelibrary.com.]

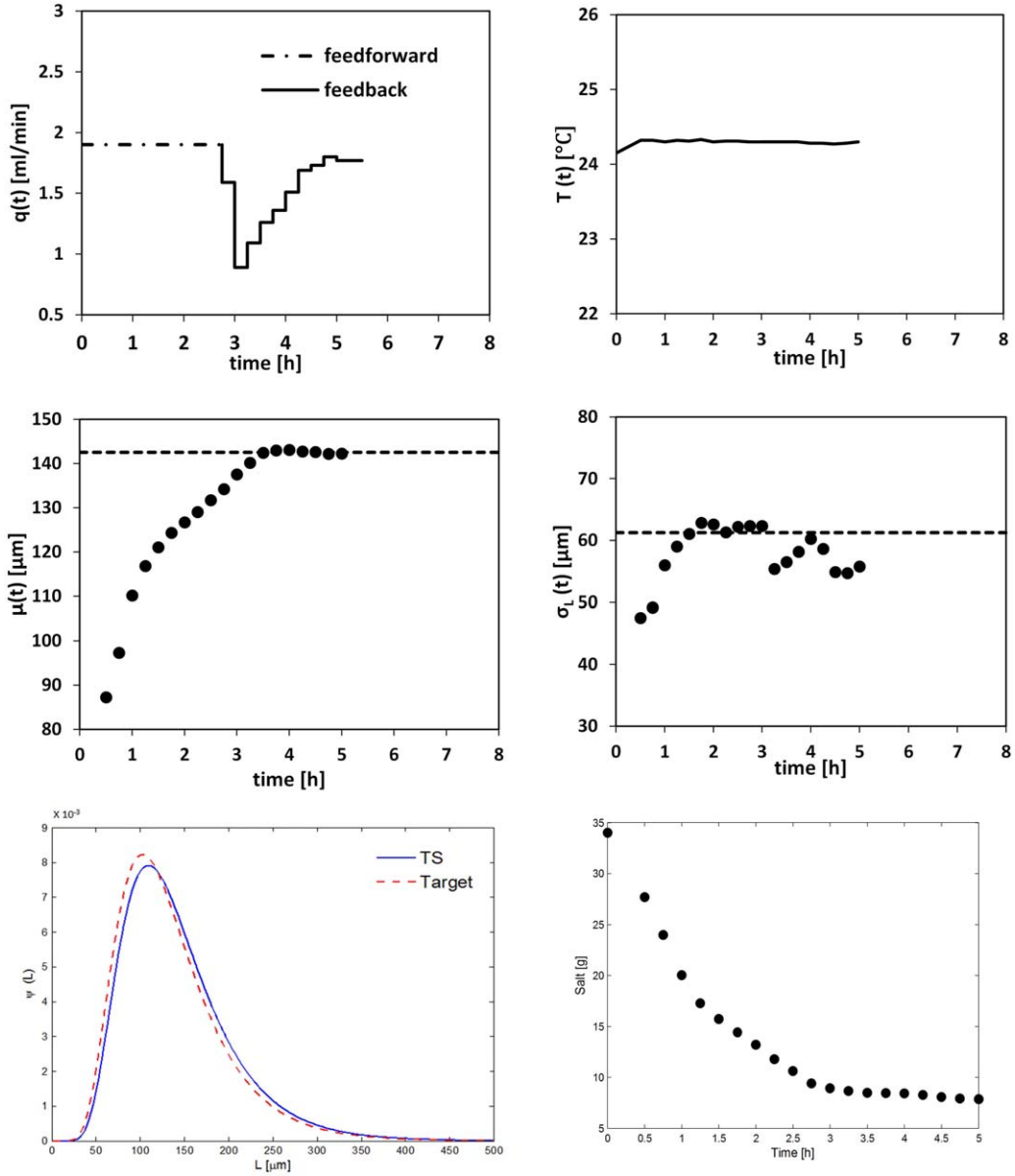

Figure 16. System behavior for FF/FB controller with the initial condition of 1.8 mL/min and 24°C for set-point.

Upper panel—Antisolvent flow rate (left) and temperature (right) profile. Middle panel—Mean (left) and standard deviation (right). Bottom panel—End of the batch distribution compared with target (left), and salt concentration profile during run (right). [Color figure can be viewed in the online issue, which is available at wileyonlinelibrary.com.]

target distributions in terms of mean and standard deviation, recalling that the two moments cannot be selected independently. *In situ* measurement of crystals' size distribution was utilized for inferring the particles characteristics captured at different time of the experiment. Digitial images were taken along the experiment. Applying a combination of thresholding and wavelet-fractal analysis images was analyzed and crystal growth were determined in automated mode.

Subsequently, alternative control strategies were implemented and tested to achieve a desired CSD. They included multiloop PIs approach, a (FF) strategy based on off-line calculated profiles and a two stages control structure using a combination of FF and FB algorithm (FF/FB). Results demonstrated in some cases poor performance of the PIs control program due to ill-conditioning of the process. Conversely, excellent behavior on the CSD control was achieved when the FF controller was applied. The two stages (FF/FB) configuration exhibited a perfect control over the mean size and it was able to achieve the asymptotic conditions faster as well as eliminating the natural effect of both model and process disturbances.

Overall, the results obtained corroborated that the FPE represents a powerful tool for antisolvent crystallization operations allowing a novel description, in a compact form, of the CSD in time and characterize the process dynamics as well as for on-line implementation of advanced control strategies. Furthermore, the implantation and testing of the proposed on-line image-based sensor provides a new direction for real-time particle characterization. Currently, there is no clear technology to directly characterize on-line CSD, especially as in the case under investigation when particles are touching and overlapping where individual particle characterization is impossible. It was shown in a bench-scale experimental setting that this methodology can solve those

problems and a completely automated system was implemented and utilized for on-line FB control of CSD.

Building on these results, this work is focusing at further uncovering the potential and expanding the capabilities of the stochastic formulation to fully characterize the dynamics involved in antisolvent mediated crystallization process. This involves the formulation and implementation strategies for on-line prediction and characterization of the CSD and solute concentration as well as model-based dynamic optimization and control studies toward fully automated operation.

Literature Cited

1. Sangwal K. *Additives and Crystallization Processes: From Fundamentals to Applications*. Chichester, England: Wiley, 2007.
2. Nagy ZK, Fujiwara M, Braatz RD. Modelling and control of combined cooling and antisolvent crystallization processes. *J Process Control*. 2008;18:856–864.
3. Widenski DJ, Abbas A, Romagnoli JA. A modeling approach for the non-isothermal antisolvent crystallization of a solute with weak temperature dependent solubility. *Cryst Res Technol*. 2012;47:491–504.
4. Sheikhzadeh M, Trifkovic M, Rohani S. Real-time optimal control of an anti-solvent semi-batch crystallization process. *Chem Eng Sci*. 2008;63:829–839.
5. Nowee SM, Abbas A, Romagnoli JA. Model-based optimal strategies for controlling particle size in anti-solvent crystallization operations. *Cryst Growth Des*. 2008;8:2698–2706.
6. Nowee SM, Abbas A, Romagnoli JA. Antisolvent crystallization: model identification, experimental validation and dynamic simulation. *Chem Eng Sci*. 2008;63:5457–5467.
7. Lindenberg C, Krattli M, Cornel J, Mazzotti M, Brozio J. Design and optimization of a combined cooling/antisolvent process. *Cryst Growth Des*. 2009;9:1124−1136.
8. Zhou GZ, Fujiwara M, Woo XY, Rusli E, Tung HH, Starbuck C, Davidson O, Ge ZH, Braatz RD. Direct design of pharmaceutical antisolvent crystallization through concentration control. *Cryst Growth Des*. 2006;6:892–898.
9. Woo XY, Nagy ZK, Tan RBH, Braatz RD. Adaptive concentration control of cooling and antisolvent crystallization with laser backscattering measurement. *Cryst Growth Des*. 2009;9:182–191.
10. Nagy ZK, Aamir E. Systematic design of supersaturation controlled crystallization processes for shaping the crystal size distribution using an analytical estimator. *Chem Eng Sci*. 2012;84:656–670.
11. Hermanto MW, Chiu MS, Woo XY, Braatz RD. Robust optimal control of polymorphic transformation in batch crystallization. *AIChE J*. 2007;53:2643–2650.
12. Abu Bakar, MR, Nagy ZK, Rielly CD. Seeded batch cooling crystallization with temperature cycling for the control of size uniformity and polymorphic purity of sulfathiazole crystals. *Org Process Res Dev*. 2009;13:1343–1356.
13. Lewiner F, Klein JP, Puel F, Fevotte G. On-line ATR FTIR measurement of supersaturation during solution crystallization processes. Calibration and applications on three solute/solvent systems. *Chem Eng Sci*. 2001;56:2069–2084.
14. Liotta V, Sabesan V. Monitoring and feedback control of supersaturation using ATR-FTIR to produce an active pharmaceutical ingredient of a desired crystal size. *Org Process Res Dev*. 2004;8:488–494.
15. Yu ZQ, Chow PS, Tan RBH. Application of attenuated total reflectance-Fourier transform infrared (ATR-FTIR) technique in the monitoring and control of anti-solvent crystallization. *Ind Eng Chem Res*. 2006;45:438–444.
16. Fujiwara M, Chow PS, Ma DL, Braatz RD. Paracetamol crystallization using laser backscattering and ATR-FTIR spectroscopy: metastability, agglomeration, and control. *Cryst Growth Des*. 2002;2:363–370.
17. Chew JW, Black SN, Chow PS, Tan RBH. Comparison between open-loop temperature control and closed-loop supersaturation control for cooling crystallization of glycine. *Ind Eng Chem Res*. 2007; 46:830–838.
18. Yu ZQ, Chew JW, Chow PS, Tan RBH. Recent advances in crystallization control—an industrial perspective. *Chem Eng Res Des*. 2007;85:893–905.
19. Lewiner F, Fevotte G, Klein J.P, Puel. Improving batch cooling seeded crystallization of an organic weed-killer using on-line ATR FTIR measurement of supersaturation. *J Cryst Growth*. 2001;226: 348–362.
20. Tadayyon A, Rohani S. Control of fines suspension density in the fines loop of a continuous KCI crystallizer using transmittance measurement and an FBRM (R) probe. *Can J Chem Eng*. 2000;78:663–673.
21. Abu Bakar MR, Nagy ZK, Saleemi AN, Rielly CD. The impact of direct nucleation control on crystal size distribution in pharmaceutical crystallization processes. *Cryst Growth Des*. 2009;9:1378–1384.
22. Abu Bakar MR, Nagy ZK, Rielly CD. Seeded batch cooling crystallization with temperature cycling for the control of size uniformity and polymorphic purity of sulfathiazole crystals. *Org Process Res Dev*. 2009;13:1343–1356.
23. Worlitschek J, Mazzotti M, Model-based optimization of particle size distribution in batch-cooling crystallization of paracetamol Processes. *Cryst Growth Des*. 2004;4:891–903.
24. Ruf A, Worlitschek J, Mazzotti M. Modeling and experimental analysis of PSD measurements through FBRM. *Part Part Syst Charact*. 2000;17:167–179.
25. Li MZ, Wilkinson D. Determination of non-spherical particle size distribution from chord length measurements. Part 1: theoretical analysis. *Chem Eng Sci*. 2005;60:3251–3265.
26. Grosso M, Galàn O, Baratti R, Romagnoli JA. A Stochastic formulation for the description of the crystal size distribution in antisolvent crystallization processes. *AIChE J*. 2010;56:2077.
27. Galan O, Grosso M, Baratti R, Romagnoli JA. Stochastic approach for the calculation of anti-solvent addition policies in crystallization operations: an application to a bench-scale semi-batch crystallizer. *Chem Eng Sci*. 2010;65:1797.
28. Cogoni G, Tronci S, Mistretta G, Baratti R, Romagnoli JA. Stochastic approach for the prediction of PSD in nonisothermal antisolvent crystallization processes. *AIChE J*. 2013;59:2843.
29. Cogoni G, Tronci S, Baratti R, Romagnoli JA. Controllability of semibatch nonisothermal antisolvent crystallization processes. *Ind Eng Chem Res*. 2014;53:7056–7065.
30. Tronci S, Grosso M, Baratti R, Romagnoli JA. A stochastic approach for the prediction of PSD in crystallization processes: analytical solution for the asymptotic behavior and parameter estimation. *Comput Chem Eng*. 2011;35:2318–2325.
31. Kumar SVS, Kumar VR, Reddy GP. Nonlinear control of bioreactors with input multiplicities: an experimental work. *Bioprocess Biosyst Eng*. 2005;28:45–53.
32. Abbas A. *A Model-Based Framework for Advanced Operation of Crystallisation Processes: A Pilot-Scale Study*. Ph.D. Thesis, Sydney, Australia: University of Sydney, 2003.
33. Nowee S.M. *Modelling and Optimization of Crystallization Processes*. Ph.D. Thesis, Sydney, Australia: University of Sydney, 2007.
34. Hayashi M. Temperature-electrical conductivity relation of water for environmental monitoring and geophysical data inversion. *Environ Monit Assess*. 2004;96:119–128.
35. Kestin J, Khalifa E, Correia RI. Tables of the dynamic and kinematic viscosity of aqueous NaCi solutions in the temperature range 20-ls00c and the pressure range 0.1–35 mpa. *J Phys Chem. Ref Data*. 1981;10:71–87.
36. Zhang B, Abbas A, Romagnoli JA. Automatic image-based estimation of texture analysis as a monitoring tool for crystal growth. *Chemometr Intell Lab Syst*. 2013;121:42–51.
37. Zhang B, Willis R, Romagnoli JA, Fois C, Tronci S, Baratti R. Image-based multiresolution-ann approach for online particle size characterization. *Ind Eng Chem Res*. 2014;53:7008–7018.
38. Velazquez-Camilo O, Bolaños-Reynoso E, Rodriguez E, Alvarez-Ramirez J. Fractal analysis of crystallization slurry images. *Cryst Growth Des*. 2010;312:842–850.
39. Grosso M, Cogoni G, Baratti R, Romagnoli JA. Stochastic approach for the prediction of PSD in crystallization processes: formulation and comparative assessment of different stochastic models. *Ind Eng Chem Res*. 2011;50:2133−2143.
40. Bonvin D. Optimal operation of batch reactors: a personal view. *J Process Control*. 1998;282:859.
41. Juba MR, Hamer JW. Progress and challenges in batch process control. In: Morari M, McAvoy TJ, editors. *Third International Conference Proceedings on Chemical Process Control*. New York: AIChE, 1986:139.

Manuscript received Oct. 2, 2014, and revision received Jan. 21, 2015.